Collaborative Calibration Algorithm in Redundant Dual-axis RINS Configuration

1st Zhonghong Liang
College of Advanced Interdisciplinary Studies
Nanhu Laser Laboratory
National University of Defense Technology
Changsha, China
lzhgzyx1@163.com

2nd Yuanhan Wang
College of Advanced Interdisciplinary Studies
Nanhu Laser Laboratory
National University of Defense Technology
Changsha, China
wyh20327@163.com

3rd Zhikun Liao
College of Advanced Interdisciplinary Studies
Nanhu Laser Laboratory
National University of Defense Technology
Changsha, China
lzkun2008@yeah.net

4th Pengcheng Mu
College of Advanced Interdisciplinary Studies
Nanhu Laser Laboratory
National University of Defense Technology
Changsha, China
pengcheng_1997@163.com

5th Hui Luo
College of Advanced Interdisciplinary Studies
Nanhu Laser Laboratory
National University of Defense Technology
Changsha, China
luohui.luo@163.com

6th Lin Wang*
College of Advanced Interdisciplinary Studies
Nanhu Laser Laboratory
National University of Defense Technology
Changsha, China
wanglin11@nudt.edu.cn

***Abstract*—Dual-axis rotational inertial navigation system (DRINS) can achieve self-calibration of error parameters to improve the navigation performance. However, the traditional self-calibration methods rely on the external reference information. This paper focuses on the dual DRINSs configuration and proposes a collaborative calibration algorithm. Considering the error parameters of redundant DRINS, the 60-D Kalman filter is established, in which the geometric constraint between systems are deployed to establish the observation equation without external reference information. A novel collaborative calibration scheme is designed based on the asynchronous rotation to make all the error states observable. Monte Carlo simulations and real system experiments are conducted to verify the effectiveness of the proposed algorithm. The result shows the algorithm works well.**

***Index Terms*—Collaborative Calibration; Redundant Dual-axis RINS; Kalman Filter;**

I. Introduction

Inertial navigation system (INS) can provide high-frequency attitude, velocity, and positioning information of the carrier in real-time. However, as a dead-reckoning autonomous navigation method, the navigation errors of INS will accumulate over time [1]. Therefore, INS works complementarily with other sensors in general, e.g. Global Navigation Satellite Systems (GNSS) [2], [3]. Nevertheless, in special scenarios, such as underwater navigation, and in GNSS-denied situations, there is no external reference information available [4]. The navigation and positioning of the carrier rely on INS. Rotational inertial navigation system (RINS) is capable of averaging out constant errors of the inertial measurement unit (IMU) through modulation technology, which can greatly enhance the accuracy of navigation performance [5], [6]. Thus, RINS has been widely used in a variety fields, especially marine navigation. According to the number of the gimbals, RINS can be divided into single-axis RINS, dual-axis RINS (DRINS) tri-axis RINS. With the development of rotational modulation technique and the improvement of inertial sensors precision, the positioning accuracy of RINS can reach 1n mile/24h even higher without the need for intervening position fixes [7], [8].

Given the high reliability requirement of navigation system for long-endurance marine, carriers are usually equipped with two or more sets of RINSs for redundant configuration [9], [10]. A redundant RINS is initially used as the hot backup to ensure that at least one RINS can still provide accurate positioning information in event of a RINS failing [11]. In most scenarios, the redundant configuration of two sets of RINS is preferable in terms of cost and reliability. Recently, there have been some studies focus on the information fusion between dual RINSs. The geometric relationship between the systems is used as the constraint observation without external reference information [12]. By designing a reasonable rotation scheme according to different system configurations, partial

error parameters of the RINSs can be estimated to improve the performance of the system [13]–[17]. Wang et al. [13] proposed a gyro drift and accelerometer bias online estimation method based on single-axis/dual-axis RINS configuration and a position error prediction model of single-axis RINS to improve the performance in the event of dual-axis RINS failure. Wu et al. [14] proposed a rotation scheme for dual DRINSs to rotate around different axes and realized on-line monitoring of inertial device biases. For two tri-axis RINSs configuration, Wu et al. [15] proposed a calibration method for inner and outer lever-arm errors utilizing the asynchronous rotation schemes of two tri-axis RINSs and carrier maneuver. This solution can also be used for dynamic calibration and compensation for gyro scale factor error of redundant fiber optics gyro (FOG) RINSs to improve the navigation accuracy [12], [16], [17].

The above methods can perform online estimation of partial error parameters without external reference information whether in static or dynamic conditions. However, all error parameters of RINS will change due to the inherent characteristics of the inertial sensor [18]. Thus, RINS need to be calibrated periodically and accurately to maintain the navigation performance. The self-calibration technology of RINS is studied to address the problem [19]. Nevertheless, the traditional self-calibration methods rely on the external reference information. In our previous paper [20], an all-parameter online calibration method is proposed based on the dual DRINSs configuration. However, this method is predicated on the assumption that the scale factor error and installation error of one set of RINS can be negligible compared to the RINS to be calibrated. On this basis, a collaborative calibration algorithm of dual DRINSs is proposed considering all error parameters of dual DRINSs. Based on the geometric constraint of dual DRINSs, a 60-D Kalman filter is established and the error parameters, including scale factor error and installation error of dual DRINSs, are well calibrated. The proposed algorithm can be used to solve the problem of DRINS calibration without external reference information in dual DRINSs configuration or the configuration with multiple DRINS.

The rest of this paper is organized as follows. In Section II, the error models of the dual DRINSs are analyzed. In Section III, the 60-D Kalman filter of collaborative calibration model is established and a novel collaborative calibration scheme is proposed based on the asynchronous rotation. In Section IV, Monte Carlo simulations and real system experiments are conducted to verify the effectiveness of the proposed calibration method. Finally, Section V concludes this article.

II. System Configuration and Error Model

A. System Configuration and Definition of the Frames

The system configuration of dual DRINSs is shown in Fig.1. DRINS k mainly consists of IMU k and two gimbals named as azimuth (inner) gimbal and roll (outer) gimbal, respectively. The IMU is installed and fixed in the inner frame. DRINS 1 and DRINS 2 are equipped on the same carrier for redundant configuration.

The definition of the frames used in this paper is shown in Table I. As shown in Fig.1, O_b and O_n are the origins of b-frame and n-frame, which are commonly located at the mass center of carrier. Due to the space limitation, the centers of two IMUs usually do not coincide with O_b and O_n, causing the outer lever-arm $\boldsymbol{l}_1$ and $\boldsymbol{l}_2$. The outer lever-arm will cause position difference and velocity difference between two DRINSs when the carrier is in angular motion. When the dual DRINSs are installed on the carrier, the spatial geometric relationship between the two systems, i.e., the outer lever-arm, is fixed and can be calibrated in advance.

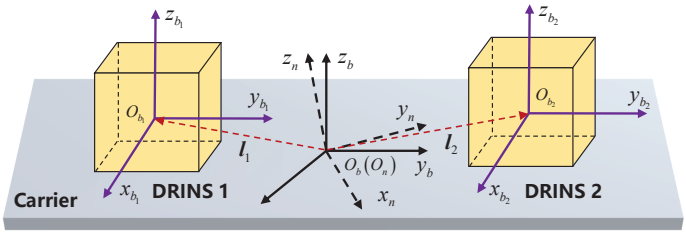

Fig. 1. System configuration

TABLE I
Frame Definition

Frames	Description
i	Inertial frame
e	Earth frame
n	Navigation frame, east-north-up
b	Body frame of the carrier, right-forward-upward
$b_k(k=1,2)$	Body frame of IMU k, right-forward-upward

B. System Error Model

1)*IMU Error Model* : Considering scale factor error, installation error, gyro drift, and accelerometer bias, the error model of gyro assembly and accelerometer assembly are respectively expressed as

$$\delta\boldsymbol{\omega}_{ib_k}^{b_k} = \delta\boldsymbol{K}_{gk}\boldsymbol{\omega}_{ib_k}^{b_k} + \boldsymbol{\varepsilon}^{b_k} + \boldsymbol{w}_g^{b_k} \tag{1}$$

$$\delta\boldsymbol{f}^{b_k} = \delta\boldsymbol{K}_{ak}\boldsymbol{f}^{b_k} + \nabla^{b_k} + \boldsymbol{w}_a^{b_k} \tag{2}$$

where $\delta\boldsymbol{\omega}_{ib_k}^{b_k}$ and $\delta\boldsymbol{f}^{b_k}$ represent the angular rate error and specific force error of gyro assembly and accelerometer assembly of DRINS k, $\boldsymbol{\omega}_{ib_k}^{b_k}$ and $\boldsymbol{f}^{b_k}$ are the true angular rate and specific force, $\boldsymbol{\varepsilon}^{b_k} = \begin{bmatrix}\varepsilon_x^{b_k} & \varepsilon_y^{b_k} & \varepsilon_z^{b_k}\end{bmatrix}^T$ is the gyro drift of DRINS k, $\nabla^{b_k} = \begin{bmatrix}\nabla_x^{b_k} & \nabla_y^{b_k} & \nabla_z^{b_k}\end{bmatrix}^T$ is the accelerometer

bias of DRINS k, $\boldsymbol{w}_a^{b_k}$ and $\boldsymbol{w}_g^{b_k}$ represent the random noise of the gyro assembly and accelerometer assembly,

$$\delta \boldsymbol{K}_{gk} = \begin{bmatrix} \delta K_{gxk} & 0 & 0 \\ \eta_{yxk} & \delta K_{gyk} & 0 \\ \eta_{zxk} & \eta_{zyk} & \delta K_{gzk} \end{bmatrix} \tag{3}$$

$$\delta \boldsymbol{K}_{ak} = \begin{bmatrix} \delta K_{axk} & \theta_{xyk} & \theta_{xzk} \\ \theta_{yxk} & \delta K_{ayk} & \theta_{yzk} \\ \theta_{zxk} & \theta_{zyk} & \delta K_{azk} \end{bmatrix} \tag{4}$$

where $\delta K_{gik}(i = x, y, z)$ is the gyro scale factor errors of DRINS k, $\delta K_{aik}(i = x, y, z)$ is the accelerometer scale factor errors of DRINS k. The installation errors of gyro assembly and accelerometer assembly are shown in Fig.2, x_{g_k}, y_{g_k}, and z_{g_k} are the tri-gyro sensitive axes. x_{a_k}, y_{a_k}, and z_{a_k} are the tri-accelerometer sensitive axes. The b_k-frame is defined as followed: x_{b_k} coinsides with x_{g_k}, y_{b_k} lies in the x_{g_k}-y_{g_k} plane, the z_{b_k} constitutes a right-handed orthogonal frame with x_{b_k} and y_{bk}. η_{yxk}, η_{zxk}, and η_{zyk} are the installation errors of gyro assembly. $\theta_{ijk}(i = x, y, z; j = x, y, z; x \neq y)$ are the installation errors of accelerometer assembly.

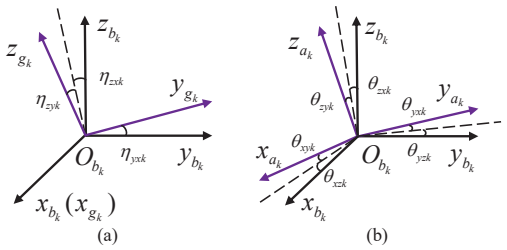

Fig. 2. Installation errors. (a) Gyro installation errors. (b) Accelerometer installation errors.

2)*Navigation Error Model* : Phi-angle error model is adopted to describe the error propagation characteristics. The error equations of dual DRINSs are expressed as

$$\dot{\boldsymbol{\phi}}_k^n = -\boldsymbol{\omega}_{in}^n \times \boldsymbol{\phi}_k^n + \delta\boldsymbol{\omega}_{in_k}^n - \boldsymbol{C}_{b_k}^n \delta\boldsymbol{\omega}_{ib_k}^{b_k} \tag{5}$$

$$\begin{aligned} \delta\dot{\boldsymbol{v}}_k^n = {} & \boldsymbol{f}^n \times \boldsymbol{\phi}_k^n - (2\boldsymbol{\omega}_{ie}^n + \boldsymbol{\omega}_{en}^n) \\ & \times \delta\boldsymbol{v}_k^n - \left(2\delta\boldsymbol{\omega}_{ie_k}^n + \delta\boldsymbol{\omega}_{en_k}^n\right) \times \boldsymbol{v}^n + \boldsymbol{C}_{b_k}^n \delta\boldsymbol{f}^{b_k} \end{aligned} \tag{6}$$

$$\begin{aligned} \delta\dot{L}_k &= \frac{1}{R_N + h}\delta v_{Nk}^n - \frac{v_N^n}{(R_E + h)^2}\delta h_k \\ \delta\dot{\lambda}_k &= \frac{v_E^n \tan L \sec L}{R_E + h}\delta L_k + \frac{\sec L}{R_E + h}\delta v_{Ek}^n - \frac{v_E^n \sec L}{(R_N + h)^2}\delta h_k \\ \delta\dot{h}_k &= \delta v_{Uk}^n \end{aligned} \tag{7}$$

with

$$\boldsymbol{\omega}_{in}^n = \boldsymbol{\omega}_{ie}^n + \boldsymbol{\omega}_{en}^n \tag{8}$$

$$\boldsymbol{\omega}_{ie}^n = \begin{bmatrix} 0 & \omega_{ie} sinL & \omega_{ie} cosL \end{bmatrix}^T \tag{9}$$

$$\boldsymbol{\omega}_{en}^n = \begin{bmatrix} -\dfrac{v_N^n}{R_N + h} & \dfrac{v_E^n \tan L}{R_E + h} & \dfrac{v_E^n}{R_E + h} \end{bmatrix}^T \tag{10}$$

where $\boldsymbol{\phi}_k^n = \begin{bmatrix} \phi_{Ek}^n & \phi_{Nk}^n & \phi_{Uk}^n \end{bmatrix}^T$ is the attitude error of DRINS k, $\boldsymbol{\omega}_{in}^n$ is the angular velocity of the n-frame relative to the i-frame, $\boldsymbol{C}_{b_k}^n$ is the direction cosine matrix from b_k-frame to n-frame, $\boldsymbol{v}^n = \begin{bmatrix} v_E^n & v_N^n & v_U^n \end{bmatrix}^T$ is the velocity of the carrier, $\delta\boldsymbol{v}_k^n = \begin{bmatrix} \delta v_{Ek}^n & \delta v_{Nk}^n & \delta v_{Uk}^n \end{bmatrix}^T$ is the velocity error of DRINS k, w_{ie}^n is the earth rotation rate, w_{en}^n is the transportation rate, L, λ, and h are the latitude, longitude, and height, respectively, δL_k, $\delta\lambda_k$, and δh_k are the latitude error, longitude error, and height error of DRINS k.

III. Collaborative Calibration Algorithm for Dual DRINSs

A. Collaborative Calibration Algorithm Overview

A Kalman filter is designed to estimate and compensate the error parameters of dual DRINSs. According to the error equations, the state equation can be established. The navigation information output from the dual DRINSs essentially reflects the motion of the same carrier, which constitutes geometric constraint observation of the error states. The calibration scheme should be designed to make all error parameters observable. The algorithm flowchart is shown in Fig.3.

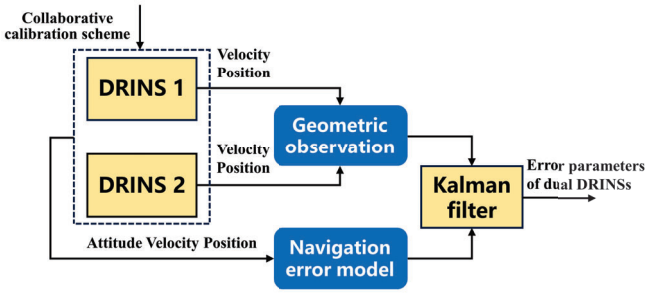

Fig. 3. Algorithm flowchart.

B. Collaborative Calibration Kalman Filter Design

1)*State Equation* : Based on the analysis in Section II, the attitude error, velocity error, position error, gyro drift, accelerometer bias, scale factor error, and installation error of dual DRINSs are considered to form 60-D state variables. According to (5)-(7), the state equation of the continuous system can be represented as

$$\dot{\boldsymbol{X}} = \boldsymbol{F}\boldsymbol{X} + \boldsymbol{G}\boldsymbol{w} \tag{11}$$

where $\boldsymbol{F}$ denotes the state transfer matrix. The details of $\boldsymbol{F}$ are shown in (11a)-(11g). The process noise matrix $\boldsymbol{G}$ is

$$\boldsymbol{G} = \begin{bmatrix} -\boldsymbol{C}_{b_1}^n & \boldsymbol{0}_{3\times3} & \boldsymbol{0}_{3\times3} & \boldsymbol{0}_{3\times3} \\ \boldsymbol{0}_{3\times3} & \boldsymbol{C}_{b_1}^n & \boldsymbol{0}_{3\times3} & \boldsymbol{0}_{3\times3} \\ \boldsymbol{0}_{3\times3} & \boldsymbol{0}_{3\times3} & \boldsymbol{0}_{3\times3} & \boldsymbol{0}_{3\times3} \\ \boldsymbol{0}_{3\times3} & \boldsymbol{0}_{3\times3} & -\boldsymbol{C}_{b_2}^n & \boldsymbol{0}_{3\times3} \\ \boldsymbol{0}_{3\times3} & \boldsymbol{0}_{3\times3} & \boldsymbol{0}_{3\times3} & \boldsymbol{C}_{b_2}^n \\ \boldsymbol{0}_{45\times3} & \boldsymbol{0}_{45\times3} & \boldsymbol{0}_{45\times3} & \boldsymbol{0}_{45\times3} \end{bmatrix} \tag{12}$$

$\boldsymbol{w}$ represents the process noise vector and is expressed as

$$\boldsymbol{w} = \begin{bmatrix} (\boldsymbol{w}_g^{b_1})^T & (\boldsymbol{w}_a^{b_1})^T & (\boldsymbol{w}_g^{b_2})^T & (\boldsymbol{w}_a^{b_2})^T \end{bmatrix}^T \tag{13}$$

$$\begin{aligned}\boldsymbol{X} = [\ & \phi_{E1}^n \quad \phi_{N1}^n \quad \phi_{U1}^n \quad \delta v_{E1}^n \quad \delta v_{N1}^n \quad \delta v_{U1}^n \quad \delta L_1 \quad \delta\lambda_1 \quad \delta h_1 \quad \varepsilon_x^{b_1} \quad \varepsilon_y^{b_1} \quad \varepsilon_z^{b_1} \quad \nabla_x^{b_1} \quad \nabla_y^{b_1} \quad \nabla_z^{b_1} \\ & \phi_{E2}^n \quad \phi_{N2}^n \quad \phi_{U2}^n \quad \delta v_{E2}^n \quad \delta v_{N2}^n \quad \delta v_{U2}^n \quad \delta L_2 \quad \delta\lambda_2 \quad \delta h_2 \quad \varepsilon_x^{b_2} \quad \varepsilon_y^{b_2} \quad \varepsilon_z^{b_2} \quad \nabla_x^{b_2} \quad \nabla_y^{b_2} \quad \nabla_z^{b_2} \\ & \delta K_{gx1} \quad \eta_{yx1} \quad \eta_{zx1} \quad \delta K_{gy1} \quad \eta_{zy1} \quad \delta K_{gz1} \quad \delta K_{ax1} \quad \theta_{yx1} \quad \theta_{zx1} \quad \theta_{xy1} \quad \delta K_{ay1} \quad \theta_{zy1} \quad \theta_{xz1} \quad \theta_{yz1} \quad \delta K_{az1} \\ & \delta K_{gx2} \quad \eta_{yx2} \quad \eta_{zx2} \quad \delta K_{gy2} \quad \eta_{zy2} \quad \delta K_{gz2} \quad \delta K_{ax2} \quad \theta_{yx2} \quad \theta_{zx2} \quad \theta_{xy2} \quad \delta K_{ay2} \quad \theta_{zy2} \quad \theta_{xz2} \quad \theta_{yz2} \quad \delta K_{az2}\ ]^T \end{aligned} \tag{11a}$$

$$\boldsymbol{F} = \begin{bmatrix} \boldsymbol{\omega}_{in}^n\times & \boldsymbol{F}_{av} & \boldsymbol{F}_{ap} & -\boldsymbol{C}_{b_1}^n & \mathbf{0}_{3\times3} & \mathbf{0}_{3\times3} & \mathbf{0}_{3\times3} & \mathbf{0}_{3\times3} & \mathbf{0}_{3\times3} & \mathbf{0}_{3\times3} & \boldsymbol{F}_{g1} & \mathbf{0}_{3\times9} & \mathbf{0}_{3\times6} & \mathbf{0}_{3\times9} \\ \boldsymbol{f}^n\times & \boldsymbol{F}_{vv} & \boldsymbol{F}_{vp} & \mathbf{0}_{3\times3} & \boldsymbol{C}_{b_1}^n & \mathbf{0}_{3\times3} & \mathbf{0}_{3\times3} & \mathbf{0}_{3\times3} & \mathbf{0}_{3\times3} & \mathbf{0}_{3\times3} & \mathbf{0}_{3\times6} & \boldsymbol{F}_{a1} & \mathbf{0}_{3\times6} & \mathbf{0}_{3\times9} \\ \mathbf{0}_{3\times3} & \boldsymbol{F}_{pv} & \boldsymbol{F}_{pp} & \mathbf{0}_{3\times3} & \mathbf{0}_{3\times3} & \mathbf{0}_{3\times3} & \mathbf{0}_{3\times3} & \mathbf{0}_{3\times3} & \mathbf{0}_{3\times3} & \mathbf{0}_{3\times3} & \mathbf{0}_{3\times6} & \mathbf{0}_{3\times9} & \mathbf{0}_{3\times6} & \mathbf{0}_{3\times9} \\ \mathbf{0}_{3\times3} & \mathbf{0}_{3\times3} & \mathbf{0}_{3\times3} & \mathbf{0}_{3\times3} & \mathbf{0}_{3\times3} & \boldsymbol{\omega}_{in}^n\times & \boldsymbol{F}_{av} & \boldsymbol{F}_{ap} & -\boldsymbol{C}_{b_2}^n & \mathbf{0}_{3\times3} & \mathbf{0}_{3\times6} & \mathbf{0}_{3\times9} & \boldsymbol{F}_{g2} & \mathbf{0}_{3\times9} \\ \mathbf{0}_{3\times3} & \mathbf{0}_{3\times3} & \mathbf{0}_{3\times3} & \mathbf{0}_{3\times3} & \mathbf{0}_{3\times3} & \boldsymbol{f}^n\times & \boldsymbol{F}_{vv} & \boldsymbol{F}_{vp} & \mathbf{0}_{3\times3} & \boldsymbol{C}_{b_2}^n & \mathbf{0}_{3\times6} & \mathbf{0}_{3\times9} & \mathbf{0}_{3\times6} & \boldsymbol{F}_{a2} \\ \mathbf{0}_{3\times3} & \mathbf{0}_{3\times3} & \mathbf{0}_{3\times3} & \mathbf{0}_{3\times3} & \mathbf{0}_{3\times3} & \mathbf{0}_{3\times3} & \boldsymbol{F}_{pv} & \boldsymbol{F}_{pp} & \mathbf{0}_{3\times3} & \mathbf{0}_{3\times3} & \mathbf{0}_{3\times6} & \mathbf{0}_{3\times9} & \mathbf{0}_{3\times6} & \mathbf{0}_{3\times9} \\ & & & & & & \mathbf{0}_{42\times62} & & & & & & & \end{bmatrix} \tag{11b}$$

$$\boldsymbol{F}_{av} = \boldsymbol{M}_1, \boldsymbol{F}_{ap} = \boldsymbol{M}_2 + \boldsymbol{M}_3, \boldsymbol{F}_{vv} = (\boldsymbol{v}^n\times)\,\boldsymbol{M}_1 - [(2\boldsymbol{\omega}_{ie}^n + \boldsymbol{\omega}_{en}^n)\times], \boldsymbol{F}_{vp} = (\boldsymbol{v}^n\times)\,(2\boldsymbol{M}_2 + \boldsymbol{M}_3) \tag{11c}$$

$$\boldsymbol{M}_1 = \begin{bmatrix} 0 & -\dfrac{1}{R_N+h} & 0 \\ \dfrac{1}{R_E+h} & 0 & 0 \\ \dfrac{\tan L}{R_E+h} & 0 & 0 \end{bmatrix}, \boldsymbol{M}_2 = \begin{bmatrix} 0 & 0 & 0 \\ -\omega_{ie}\sin L & 0 & 0 \\ \omega_{ie}\cos L & 0 & 0 \end{bmatrix}, \boldsymbol{M}_3 = \begin{bmatrix} 0 & 0 & \dfrac{v_N^n}{(R_E+h)^2} \\ 0 & 0 & -\dfrac{v_E^n}{(R_E+h)^2} \\ \dfrac{v_E^n\sec^2 L}{R_E+h} & 0 & -\dfrac{v_E^n\tan L}{(R_E+h)^2} \end{bmatrix} \tag{11d}$$

$$\boldsymbol{F}_{pv} = \begin{bmatrix} 0 & \dfrac{1}{R_N+h} & 0 \\ \dfrac{\sec L}{R_E+h} & 0 & 0 \\ 0 & 0 & 1 \end{bmatrix}, \boldsymbol{F}_{pp} = \begin{bmatrix} 0 & 0 & \dfrac{-v_N}{(R_N+h)^2} \\ \dfrac{v_E\sec L\tan L}{R_E+h} & 0 & \dfrac{-v_E\sec L}{(R_E+h)^2} \\ 0 & 0 & 0 \end{bmatrix} \tag{11e}$$

$$\boldsymbol{F}_{g1} = -\boldsymbol{C}_{b_1}^n \begin{bmatrix} \tilde{\omega}_{ib_1x}^{b1}\boldsymbol{I}_{3\times3} & \begin{bmatrix} \mathbf{0}_{1\times2} \\ \tilde{\omega}_{ib_1y}^{b1}\boldsymbol{I}_{2\times2} \end{bmatrix} & \begin{bmatrix} \mathbf{0}_{2\times1} \\ \tilde{\omega}_{ib_1z}^{b1} \end{bmatrix} \end{bmatrix}, \boldsymbol{F}_{a1} = \boldsymbol{C}_{b_1}^n \begin{bmatrix} \tilde{f}_x^{b1}\boldsymbol{I}_{3\times3} & \tilde{f}_y^{b1}\boldsymbol{I}_{3\times3} & \tilde{f}_z^{b1}\boldsymbol{I}_{3\times3} \end{bmatrix} \tag{11f}$$

$$\boldsymbol{F}_{g2} = -\boldsymbol{C}_{b_2}^n \begin{bmatrix} \tilde{\omega}_{ib_2x}^{b2}\boldsymbol{I}_{3\times3} & \begin{bmatrix} \mathbf{0}_{1\times2} \\ \tilde{\omega}_{ib_2y}^{b2}\boldsymbol{I}_{2\times2} \end{bmatrix} & \begin{bmatrix} \mathbf{0}_{2\times2} \\ \tilde{\omega}_{ib_2z}^{b2} \end{bmatrix} \end{bmatrix}, \boldsymbol{F}_{a2} = \boldsymbol{C}_{b_2}^n \begin{bmatrix} \tilde{f}_x^{b2}\boldsymbol{I}_{3\times3} & \tilde{f}_y^{b2}\boldsymbol{I}_{3\times3} & \tilde{f}_z^{b2}\boldsymbol{I}_{3\times3} \end{bmatrix} \tag{11g}$$

---

2)*Observation Equation* : Since the dual DRINSs are installed on the same carrier, the output navigation information of dual DRINSs reflects the motion state of same carrier. The relative geometric relationship between the two systems, also known as the outer lever-arm, is fixed and can be calibrated in advance [21]. The velocity and the position difference of dual DRINSs caused by outer lever-arm are

$$\boldsymbol{v}_{l_k}^n = \begin{bmatrix} v_{l_{Ek}}^n & v_{l_{Nk}}^n & v_{l_{Uk}}^n \end{bmatrix}^T = \boldsymbol{C}_b^n\left(\boldsymbol{\omega}_{eb}^b \times \boldsymbol{l}_k^b\right) \tag{14}$$

$$\boldsymbol{l}_{p_k} = \begin{bmatrix} l_{L_k} & l_{\lambda_k} & l_{h_k} \end{bmatrix}^T = \boldsymbol{F}_{pv}\boldsymbol{l}_k^n \tag{15}$$

The velocity and position output of DRINS k are

$$\tilde{\boldsymbol{v}}_k^n = \boldsymbol{v}^n + \boldsymbol{v}_{l_k}^n + \delta\boldsymbol{v}_k^n \tag{16}$$

$$\tilde{\boldsymbol{p}}_k = \boldsymbol{p} + \boldsymbol{l}_{p_k} + \delta\boldsymbol{p}_k \tag{17}$$

where $\boldsymbol{v}^n$ and $\boldsymbol{p}$ are the true velocity and position of the carrier, respectively. Thus, the differences of velocity error and position error between dual DRINSs are represented as

$$\delta\boldsymbol{v}_{12}^n = \left(\tilde{\boldsymbol{v}}_1^n - \boldsymbol{v}_{l_1}^n\right) - \left(\tilde{\boldsymbol{v}}_2^n - \boldsymbol{v}_{l_2}^n\right) = \tilde{\boldsymbol{v}}_{12}^n - \boldsymbol{v}_{l_{12}}^n \tag{18}$$

$$\delta\boldsymbol{p}_{12} = (\tilde{\boldsymbol{p}}_1 - \boldsymbol{l}_{p_1}) - (\tilde{\boldsymbol{p}}_2 - \boldsymbol{l}_{p_2}) = \tilde{\boldsymbol{p}}_{12} - \boldsymbol{l}_{p_{12}} \tag{19}$$

where the subscript '12' represents the difference between the corresponding vectors of dual DRINSs. For marine navigation, there is usually external height observation, such as sea level and depth gauge. The horizontal velocity difference, horizontal position difference, vertical velocity, and height are chosen as the observation. The observation equation is expressed as

$$\begin{aligned}\boldsymbol{Z} &= \boldsymbol{H}\boldsymbol{X} + \boldsymbol{v} \\ &= \begin{bmatrix} \delta v_{E12}^n & \delta v_{N12}^n & \delta v_{U1}^n & \delta v_{U2}^n & \delta L_{12} & \delta\lambda_{12} & \delta h_1 & \delta h_2 \end{bmatrix}^T \end{aligned} \tag{20}$$

with

$$\boldsymbol{H} = \begin{bmatrix} \boldsymbol{H}_{rv} & \boldsymbol{H}_v & \boldsymbol{H}_{rp} & \boldsymbol{H}_h \end{bmatrix}^T \tag{21}$$

$$\boldsymbol{H}_{rv} = \begin{bmatrix} \mathbf{0}_{2\times3} & \boldsymbol{I}_{2\times2} & \mathbf{0}_{2\times13} & -\boldsymbol{I}_{2\times2} & \mathbf{0}_{2\times40} \end{bmatrix} \tag{22}$$

$$\boldsymbol{H}_v = \begin{bmatrix} \mathbf{0}_{1\times5} & 1 & \mathbf{0}_{1\times14} & 0 & \mathbf{0}_{1\times39} \\ \mathbf{0}_{1\times5} & 0 & \mathbf{0}_{1\times14} & 1 & \mathbf{0}_{1\times39} \end{bmatrix} \tag{23}$$

$$\boldsymbol{H}_{rp} = \begin{bmatrix} \mathbf{0}_{2\times6} & \boldsymbol{I}_{2\times2} & \mathbf{0}_{2\times13} & -\boldsymbol{I}_{2\times2} & \mathbf{0}_{2\times37} \end{bmatrix} \tag{24}$$

$$\boldsymbol{H}_h = \begin{bmatrix} \mathbf{0}_{1\times8} & 1 & \mathbf{0}_{1\times14} & 0 & \mathbf{0}_{1\times36} \\ \mathbf{0}_{1\times8} & 0 & \mathbf{0}_{1\times14} & 1 & \mathbf{0}_{1\times36} \end{bmatrix} \tag{25}$$

where $\delta v_{E12}^n = \delta v_{E12}^n - \delta v_{E2}^n$ represents the difference between the velocity error of dual DRINSs and the other variables with subscripts "12" represent the difference between corresponding variables of dual DRINSs, $\boldsymbol{v}$ denotes the measurement noise vector. The time-continuous dynamic model should be discreted and the discrete method refer to [12].

C. Collaborative Calibration Scheme Design

The calibration scheme refers to the rotation sequences of the gimbals during the calibration process. The reasonable calibration scheme needs to ensure that error parameters to be calibrated of the system are excited and estimated. Therefore, the design of calibration scheme is the crucial process of the calibraiton technology. For homogeneous and isomorphic dual DRINSs, the error propagation characteristics of dual DRINSs are similar. Therefore, in order to estimate the error parameters of the two systems separately, the rotation schemes of the two systems need to be distinguished [20]. Hu et al. [22] pointed that the asynchronous rotation can enhance the installation error observability of dual RINS, and the asynchronous time is also an important factor affecting system observability. In this paper, the gyro related errors are excited by the rotation of the gimbals. Therefore, the asynchronous rotation is also necessary in collaborative calibration scheme design of dual DRINSs to estimate gyro related errors.

During the calibration process, the input of gyros is derived from the rotation of the gimbals and the input of accelerometers is the the component of gravity. In order to excite all the error parameters, each sensitive axis needs the excitation input. Therefore, the calibration scheme needs to include the rotation sequences around the tri-axis gyros and up-and-down flips of the tri-axis accelerometers. Based on the above analysis, a novel collaborative calibration scheme for dual DRINSs is proposed in Table II. The proposed calibration scheme is based on the asynchronous rotation mode, which means the dual DRINSs rotate alternately. Sequence 1 representsthe outer gimbal of DRINS 1 rotates 180°, while DRINS 2 maintains stationary. The scheme contains forward and reverse rotations around tri-axis gyros. The rotation sequences which rotates 180° around the horizontal axis achieves the up-and-down flips of the accelerometer sensitive axes and the rotation sequences which rotates 90° around the horizontal axis exchanges the rotation axis. Through the combination of these sequences, it is possible to estimate all the error parameters of the dual DRINSs utilizing the geometric constraint observation.

TABLE II
COLLABORATIVE CALIBRATION SCHEME FOR DUAL DRINSS

Sequence	DRINS 1		Sequence	DRINS 2	
	Inner gimbal	Outer gimbal		Inner gimbal	Outer gimbal
1	0°	180°	2	0°	180°
3	0°	90°	4	0°	90°
5	0°	-180°	6	0°	-180°
7	180°	0°	8	180°	0°
9	90°	0°	10	90°	0°
11	-180°	0°	12	-180°	0°
13	0°	-180°	14	0°	-180°
15	0°	-90°	16	0°	-90°
17	0°	180°	18	0°	180°
19	180°	0°	20	180°	0°
21	0°	-180°	22	0°	-180°
23	0°	-90°	24	0°	-90°
25	0°	180°	26	0°	180°
27	-180°	0°	28	-180°	0°
29	-90°	0°	30	-90°	0°
31	180°	0°	32	180°	0°
33	0°	180°	34	0°	180°
35	0°	90°	36	0°	90°
37	0°	-180°	38	0°	-180°
39	-180°	0°	40	-180°	0°

IV. SIMULATION AND EXPERIMENT RESULT AND ANALYSIS

A. Monte Carlo Simulation

Monte Carlo simulations are conducted to validate the accuracy of the proposed collaborative calibration method. The proposed calibration scheme is employed. The scale factor error, installation error, gyro drift, accelerometer bias, and random error are considered and the errors are added according to (1) and (2). The random error is modeled as the white noise, where the gyro random error is set as $0.0005°/\sqrt{h}$ and the accelerometer random error is set as $5\mu g/\sqrt{Hz}$ according to the typical accuracy of the marine DRINS. The real values of other error parameters are listed in Table III. The rotation angular velocities of the gimbals are set as 9°/s. The whole collaborative calibration process lasts 5.8 h. Since the dual-axis rotation modulation technique can effectively eliminate the influence of gyro constant drift and accelerometer constant bias on the navigation and the estimation of gyro drift needs a complex rotation process with long estimation time [21], only scale factor errors and installation errors are considered in experiments to simplify the analysis. Fifty times simulations are performed. The convergence curves of error parameters of the 50 experiments are shown in Fig.4 - Fig.7.

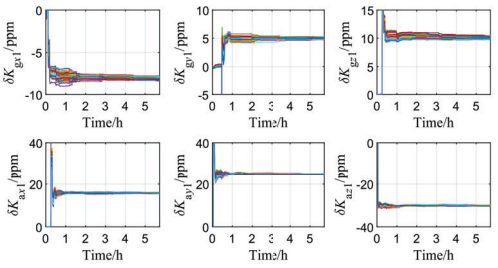

Fig. 4. Scale factor error of DRINS 1.

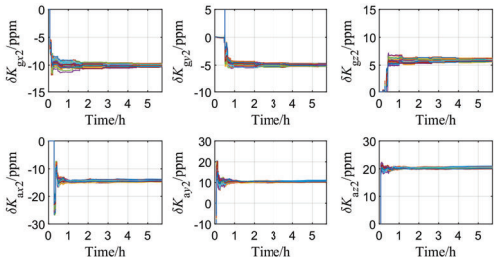

Fig. 5. Scale factor errors of DRINS 2.

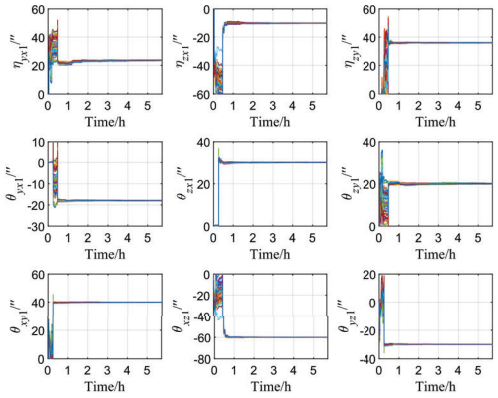

Fig. 6. Installation error of DRINS 1.

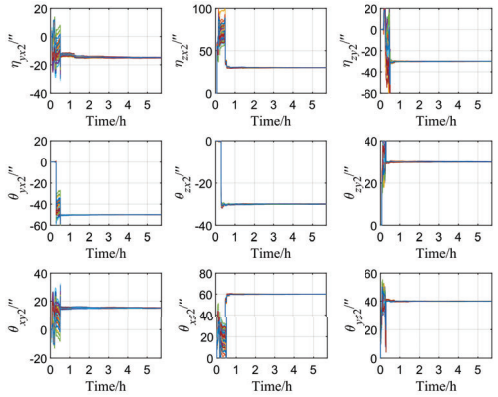

Fig. 7. Installation error of DRINS 2.

TABLE III

STATISTIC RESULTS OF THE SIMULATIONS

Error Parameters	DRINS1			DRIN2		
	Real Value	Error (RMSE)	Error (Max)	Real Value	Error (RMSE)	Error (Max)
δK_{gxk}/ppm	-8	0.17	0.43	-10	0.17	0.51
δK_{gyk}/ppm	5	0.14	0.36	-5	0.15	0.42
δK_{gzk}/ppm	10	0.20	0.50	6	0.20	0.44
δK_{axk}/ppm	16	0.35	0.64	-15	0.50	0.99
δK_{ayk}/ppm	25	0.43	0.81	30	0.51	0.88
δK_{azk}/ppm	-30	0.48	0.98	-30	0.43	0.91
$\eta_{yxk}/''$	24	0.30	0.57	16	0.22	0.51
$\eta_{zxk}/''$	-10	0.12	0.45	25	0.11	0.30
$\eta_{zyk}/''$	36	0.11	0.27	-30	0.10	0.28
$\theta_{yxk}/''$	-18	0.09	0.18	-50	0.09	0.23
$\theta_{zxk}/''$	30	0.06	0.16	-30	0.06	0.19
$\theta_{zyk}/''$	40	0.06	0.15	30	0.07	0.18
$\theta_{xyk}/''$	20	0.17	0.48	15	0.21	0.43
$\theta_{xzk}/''$	-60	0.09	0.27	60	0.08	0.20
$\theta_{yzk}/''$	-30	0.08	0.19	40	0.08	0.20

As shown in Fig.4 - Fig.7, all error parameters converge around the setting values, which indicates that the proposed algorithm can achieve the calibration of all error parameters without external reference information and the algorithm has good repeatability.

The statistic results, including the root mean square error and the maximum error of the Monte Carlo simulations are listed in Table III. The result shows that the calibration accuracy of the proposed algorithm is pretty high which can meet the needs of long-endurance marine navigation. After the collaborative calibration of dual DRINSs, the gyro scale factor error is less than 0.2 ppm (1σ), the accelerometer scale factor error less than 0.6 ppm (1σ), the installation error less than $0.3''$ (1σ).

B. Real System Experiment

In order to further verify the effectiveness of the proposed algorithm, the real system experiment has been conducted. The experimental system is shown in Fig.8. The inertial sensors of IMU includes tri-axis ring laser gyros and tri-axis quartz accelerometers. The gyro drift stability is less than 0.003 °/h and the accelerometer bias stability is less than 20 μg. Two IMUs and the turntable form the dual DRINSs in this experiment. Since the two IMUs are installed in the same location and the experiment is conducted in static condition, the error caused by outer lever-arm can be ignored. The calibration experiments of the two IMUs are conducted on the turntable at different times, and the collaborative calibration of the two systems is performed by aligning time stamps.

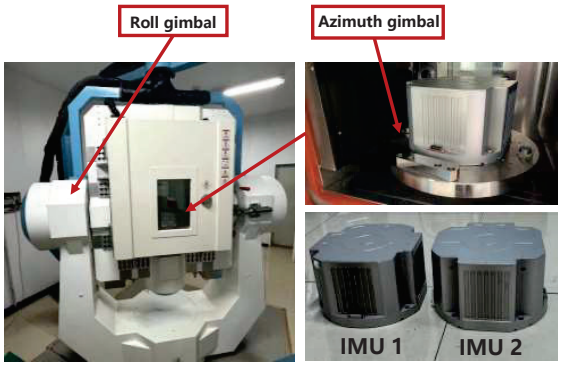

Fig. 8. Experimental system.

Since the real value of system error parameters cannot be obtained, the traditional system-level calibration method is used to accurately calibrated the system errors, and then the known errors are added. The calibration accuracy is evaluated by comparing the estimated value of errors obtained from the collaborative calibration algorithm with the added errors. The value of added errors are same as the simulation, and it is shown in Table III. The convergence curves of error parameters are shown in Fig.9 - Fig.10.

In Fig.9 - Fig.10, the black dashed lines indicate the value of added errors and the results show that the scale factor error and installation error converges to near the added value. To assess the repeatability of the collaborative calibration algorithm, the experiments are conducted three times under identical conditions. The calibration results of three tests are given in Table IV and Table V.

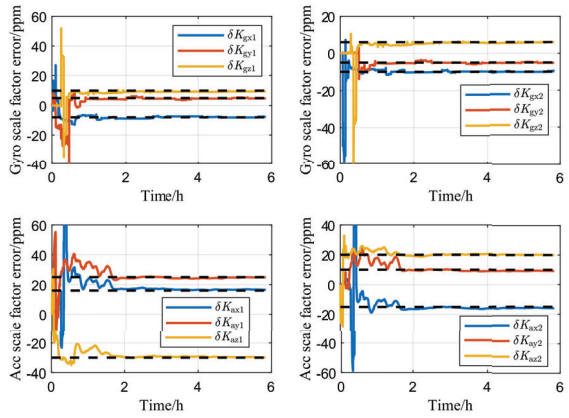

Fig. 9. Scale factor error estimation.

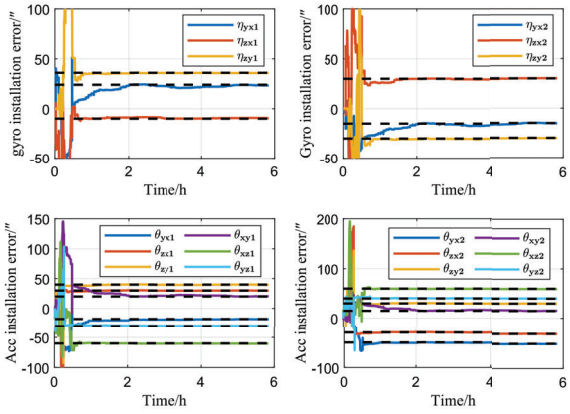

Fig. 10. Installation error estimation.

TABLE IV

CALIBRATION RESULTS OF DRINS 1

Error Parameters	Real Value	Calibration Errors of DRINS 1			
		Test 1	Test 2	Test 3	RMS
δK_{gx1}/ppm	-8	0.28	0.42	-0.05	0.29
δK_{gy1}/ppm	5	-0.25	-0.27	-0.34	0.29
δK_{gz1}/ppm	10	-0.44	0.08	-0.24	0.29
δK_{ax1}/ppm	16	0.54	0.44	0.82	0.62
δK_{ay1}/ppm	25	-0.12	-1.41	-0.22	0.83
δK_{az1}/ppm	-30	0.19	-0.15	-0.37	0.26
$\eta_{yx1}/''$	24	-0.70	-0.27	-0.41	0.49
$\eta_{zx1}/''$	-10	0.41	0.22	0.08	0.27
$\eta_{zy1}/''$	36	-0.17	0.18	-0.86	0.52
$\theta_{yx1}/''$	-18	-0.21	0.37	-0.63	0.44
$\theta_{zx1}/''$	30	-0.04	0.01	-0.06	0.05
$\theta_{zy1}/''$	40	-0.19	-0.29	-0.23	0.24
$\theta_{xy1}/''$	20	0.48	-0.13	0.18	0.30
$\theta_{xz1}/''$	-60	-0.46	-0.43	-0.18	0.38
$\theta_{yz1}/''$	-30	0.38	0.35	1.12	0.71

As shown in Table IV and Table V, the proposed algorithm shows good performance in three tests. The root mean square

TABLE V

CALIBRATION RESULTS OF DRINS 2

Error Parameters	Real Value	Calibration Errors of DRINS 2			
		Test 1	Test 2	Test 3	RMS
δK_{gx2}/ppm	-10	0.11	0.42	0.26	0.29
δK_{gy2}/ppm	-5	-0.23	-0.12	-0.37	0.26
δK_{gz2}/ppm	6	-0.02	0.24	-0.04	0.14
δK_{ax2}/ppm	-15	-0.94	-0.06	-0.19	0.55
δK_{ay2}/ppm	30	-0.81	0.43	-0.17	0.54
δK_{az2}/ppm	-30	-0.01	0.60	0.08	0.35
$\eta_{yx2}/''$	16	-0.25	-0.16	-0.59	0.38
$\eta_{zx2}/''$	25	-0.02	0.33	-0.16	0.21
$\eta_{zy2}/''$	-30	-0.24	-0.63	-0.87	0.63
$\theta_{yx2}/''$	-50	-0.46	-0.43	-0.59	0.50
$\theta_{zx2}/''$	-30	-0.13	-0.09	-0.18	0.14
$\theta_{zy2}/''$	30	-0.08	0.02	-0.10	0.07
$\theta_{xy2}/''$	15	0.47	0.58	0.85	0.65
$\theta_{xz2}/''$	60	-0.45	-0.29	-0.20	0.33
$\theta_{yz2}/''$	40	0.40	0.53	0.74	0.57

(RMS) of gyro scale factor error, accelerometer error, and installation error are less than 0.3 ppm, 0.9 ppm, and $0.8''$. The estimation accuracy of the real system experiment is slightly lower compared to the simulation results. This discrepancy arises from the presence of residual errors that persist even after compensating for the error parameters. Consequently, these residual errors become coupled in the calibration results.

V. CONCLUSIONS

A collaborative calibration algorithm based on geometric constraint is proposed in this paper. Based on the analysis of error model of dual DRINSs, the 60-D Kalman filter is established. The geometric relationship of dual DRINSs is deployed to establish the observation equation. A collaborative calibration sheme is designed based on the asynchronous rotation. The validity of the calibration algorithm is tested by both Monte Carlo simulation and real system experiment. It can be seen from the experiment result that the proposed algorithm can effectively calibrate the error parameters of the redundant DRINS. This algorithm can effectively solve the calibration problem of DRINS without external information. Since the geometric relationship is used as the observation, the calibration can be realized either in swaying or dynamic conditions. In our future work, we will conduct a more comprehensive investigation into the impact of other errors on the algorithm, aiming to enhance the calibration accuracy even further.

REFERENCES

[1] B. Wang, Q. Ren, Z. Deng, and M. Fu, "A self-calibration method for nonorthogonal angles between gimbals of rotational inertial navigation

system," *IEEE Transactions on Industrial Electronics*, vol. 62, no. 4, pp. 2353–2362, 2014.

[2] Y. Wu, J. Wang, and D. Hu, "A new technique for ins/gnss attitude and parameter estimation using online optimization," *IEEE Transactions on Signal Processing*, vol. 62, no. 10, pp. 2642–2655, 2014.

[3] J. Tang, H. Bian, H. Ma, and R. Wang, "Sins/gnss integrated navigation based on invariant error models in inertial frame," *IEEE Sensors Journal*, vol. 24, no. 4, pp. 4290–4303, 2024.

[4] W. Ouyang, Y. Wu, and H. Chen, "Ins/odometer land navigation by accurate measurement modeling and multiple-model adaptive estimation," *IEEE Transactions on Aerospace and Electronic Systems*, vol. 57, no. 1, pp. 245–262, 2020.

[5] S. Ishibashi, S. Tsukioka, H. Yoshida, T. Hyakudome, T. Sawa, J. Tahara, T. Aoki, and A. Ishikawa, "Accuracy improvement of an inertial navigation system brought about by the rotational motion," in *Oceans 2007-Europe*. IEEE, 2007, pp. 1–5.

[6] F. Zha, L. Chang, and H. He, "Comprehensive error compensation for dual-axis rotational inertial navigation system," *IEEE Sensors Journal*, vol. 20, no. 7, pp. 3788–3802, 2020.

[7] T. Tucker and E. Levinson, "The an/wsn-7b marine gyrocompass/navigator," in *Proceedings of the 2000 national technical meeting of the institute of navigation*, 2000, pp. 348–357.

[8] E. Levinson, J. Ter Horst, and M. Willcocks, "The next generation marine inertial navigator is here now," in *Proceedings of 1994 IEEE Position, Location and Navigation Symposium-PLANS'94*. IEEE, 1994, pp. 121–127.

[9] J. Bird and J. McMillan, "A dual inertial integrated navigation system," in *Proceedings of the 54th Annual Meeting of The Institute of Navigation (1998)*, 1998, pp. 373–382.

[10] E. Levinson and R. Majure, "Accuracy enhancement techniques applied to the marine ring laser inertial navigator (marlin)," *Navigation*, vol. 34, no. 1, pp. 64–86, 1987.

[11] L. Wang, W. Wu, J. Lian, and X. Kong, "Redundant rins information fusion with application to shipborne transfer alignment," in *2018 21st International Conference on Information Fusion (FUSION)*. IEEE, 2018, pp. 2246–2253.

[12] J. Cui, W. Wu, T. Ma, M. Wang, and C. Ji, "A novel co-calibration method for a dual heterogeneous redundant marine ins," *NAVIGATION: Journal of the Institute of Navigation*, vol. 70, no. 4, p. /navi.620, 2023.

[13] L. Wang, W. Wu, G. Wei, X. Pan, and J. Lian, "Navigation information fusion in a redundant marine rotational inertial navigation system configuration," *The Journal of Navigation*, vol. 71, no. 6, pp. 1531–1552, 2018.

[14] Q. Wu and K. Li, "An inertial device biases on-line monitoring method in the applications of two rotational inertial navigation systems redundant configuration," *Mechanical Systems and Signal Processing*, vol. 120, pp. 133–149, 2019.

[15] Q. Wu, K. Li, and T. Song, "The calibration for inner and outer lever-arm errors based on velocity differences of two rinss," *Mechanical Systems and Signal Processing*, vol. 160, p. 107868, 2021.

[16] H. Han, L. Wang, and M. Wang, "A dynamic gyro scale factor error calibration method for rinss," *IEEE Sensors Journal*, vol. 21, no. 18, pp. 20 817–20 823, 2021.

[17] M. Wang, L. Wang, and H. Han, "Research on improving heading and attitudes accuracy by online calibration of errors based on multi-rinss joint rotation modulation," *IEEE Sensors Journal*, vol. 22, no. 5, pp. 4503–4513, 2022.

[18] Q. Ren, B. Wang, Z. Deng, and M. Fu, "A multi-position self-calibration method for dual-axis rotational inertial navigation system," *Sensors and Actuators A: Physical*, vol. 219, pp. 24–31, 2014.

[19] Z. Wen, G. Yang, Q. Cai, and T. Chen, "An encoder-based relative attitude observation method for self-calibration in dual-axis rins," *IEEE Transactions on Industrial Electronics*, 2022.

[20] Z. Liang, h. Luo, L. Ding, W. Guo, Y. xudong, and W. lin, "All-parameter online calibration algorithm based on the information collaboration between two inertial navigation systems," *Journal of Chinese Inertial Technology*, vol. 31, no. 4, pp. 319–326, 2023.

[21] X. Hu, Z. Wang, H. Weng, and X. Zhao, "Self-calibration of tri-axis rotational inertial navigation system based on virtual platform," *IEEE Transactions on Instrumentation and Measurement*, vol. 70, pp. 1–10, 2021.

[22] P. Hu, P. Xu, B. Chen, and Q. Wu, "A self-calibration method for the installation errors of rotation axes based on the asynchronous rotation of rotational inertial navigation systems," *IEEE Transactions on Industrial Electronics*, vol. 65, no. 4, pp. 3550–3558, 2017.